

Sharpness-Aware Minimization with Adaptive Regularization for Training Deep Neural Networks

Jinping Zou, Xiaoge Deng*, and Tao Sun*

College of Computer Science and Technology, National University of Defense Technology, Changsha, China

Emails: {zoujinping, dengxg}@nudt.edu.cn, suntao.saltfish@outlook.com

Abstract—Sharpness-Aware Minimization (SAM) has proven highly effective in improving model generalization in machine learning tasks. However, SAM employs a fixed hyperparameter associated with the regularization to characterize the sharpness of the model. Despite its success, research on adaptive regularization methods based on SAM remains scarce. In this paper, we propose the SAM with Adaptive Regularization (SAMAR), which introduces a flexible sharpness ratio rule to update the regularization parameter dynamically. We provide theoretical proof of the convergence of SAMAR for functions satisfying the Lipschitz continuity. Additionally, experiments on image recognition tasks using CIFAR-10 and CIFAR-100 demonstrate that SAMAR enhances accuracy and model generalization.

Index Terms—Sharpness-Aware Minimization, Adaptive Regularization, Nonconvex Optimization Method, Algorithm Convergence Analysis

I. INTRODUCTION

Since the introduction of Sharpness-Aware Minimization (SAM) by [6], it has garnered significant attention in machine learning. SAM is a novel and effective method for training overparameterized models and improving generalization performance. By minimizing the maximum loss within the neighborhood of model parameter spaces, SAM achieves a smoother and flatter loss surface, leading to enhanced generalization. SAM can be viewed as a variant of Stochastic Gradient Descent (SGD), where a fixed hyperparameter is used to capture the sharpness property of the model through regularization. This naturally raises the following question:

Can we develop a SAM method with adaptive regularization to further improve the generalization?

Despite extensive research on SAM and adaptive methods, no existing studies or algorithms have addressed SAM-based adaptive regularization to the best of our knowledge. To fill this gap, we propose the SAM with Adaptive Regularization (SAMAR) algorithm. This paper answers the posed question by showing that SAMAR can adaptively adjust regularization parameter based on sharpness information from the loss surface.

A. Contributions

The main contributions of this paper are as follows:

*Corresponding authors. This work is sponsored in part by the National Natural Science Foundation of China under Grant 62376278, Hunan Provincial Natural Science Foundation of China (No. 2022JJ10065), Young Elite Scientists Sponsorship Program by CAST (No. 2022QNRC001), Continuous Support of PDL (No. WDZC20235250101).

- 1) We propose a novel variant of the SAM algorithm, SAMAR, which incorporates adaptive regularization. SAMAR adjusts the regularization parameter dynamically based on the ratio of sharpness between successive iterations, leading to better generalization performance.
- 2) We provide a theoretical convergence analysis of SAMAR, showing that it achieves a sublinear convergence rate of $\mathcal{O}(1/\sqrt{K})$.
- 3) Through empirical experiments on the CIFAR-10 and CIFAR-100 datasets, we demonstrate that SAMAR outperforms other optimizers in terms of accuracy and generalization.

B. More Related Works

Adaptive Sharpness-Aware Minimization (ASAM), introduced by [13], incorporates normalization operations and adaptive sharpness to demonstrate that adaptive sharpness exhibits scale-invariant properties. It also shows that adaptive sharpness correlates more strongly with generalization compared to sharpness defined in a fixed-radius spherical region. The authors also provide ASAM’s generalization bound derived from the PAC-Bayesian framework, which closely aligns with those of SAM. Several variants of SAM and ASAM have since been developed. Li et al. [14] introduce the Variance-Suppressed Sharpness-Aware Optimization (VaSSO) scheme, which enhances model stability by reducing the mean square error in the stochastic direction. They define a new δ -stability measure to assess the effect of stochastic linearization. Liu et al. [17] propose the LookSAM and Look-LayerSAM algorithms. LookSAM reduces computational overhead by leveraging the fact that \mathbf{g}_v , the orthogonal component of SAM’s gradient \mathbf{g}_s relative to SGD’s gradient \mathbf{g}_h , changes slowly, thus allowing for periodic computation of SAM’s gradient. Look-LayerSAM scales up the batch size to 64K for large-batch training. Li et al. [15] present FSAM and reveal that stochastic gradient noise plays a role in improving generalization by decomposing the sample gradient. Mi et al. [18] propose SSAM, a method with sparse perturbations generated from a binary mask based on Fisher information and dynamic sparse training. Andriushchenko et al. [2] offer a comprehensive understanding toward SAM and explain why SAM converges a solution with better generalization performance. Jiang et al. [9] investigate 40 complexity measures and suggest that sharpness-based measures correlate highly with generalization ability. Shirish Keskar et al. [10] show that large-

batch methods converge to sharp minimizers with poorer generalization and small-batch methods converge consistently to flat minimizers with better generalization. They attribute this discrepancy to the inherent noise in the gradient estimation. Khanh et al. [11] provide detailed analysis and rigorous proofs of SAM’s convergence for convex and nonconvex objectives.

In addition to these approaches, there are several powerful methods aimed at improving neural network training and reducing generalization error, such as Adaptive Stochastic Gradient Descent (ASGD) [20, 22], the Momentum method [19, 21, 23], adaptive step-size methods [16], the Heavy Ball (HB) algorithm [24], and various regularization methods [1, 3, 12]. For example, Bellavia et al. [3] construct a third-order polynomial model with an adaptive regularization term σ_k , using inexact gradient estimates and Hessian information. They show that the expected number of iterations to reach an ϵ -approximation of the first-order stationary point is at most $\mathcal{O}(\epsilon^{-3/2})$. Agarwal et al. [1] extend Adaptive Regularization Cubics (ARC) to optimization on Riemannian manifolds, updating σ_k with a more flexible rule. Bottou et al. [4] provide a comprehensive overview of optimization theory in machine learning, offering a holistic view of key methods such as stochastic gradient methods, first-order and second-order regularization techniques, and accelerated gradient methods.

II. METHODOLOGY

A. Sharpness-Aware Minimization with Adaptive Regularization

Our focus is on solving the empirical risk minimization problem in machine learning, which could be formally described as the following process

$$\min_{\mathbf{x} \in \mathbb{R}^d} f(\mathbf{x}) \triangleq \frac{1}{n} \sum_{i=1}^n f_i(\mathbf{x}), \text{ where } f_i(\mathbf{x}) \triangleq \ell(h(s_i; \mathbf{x}), y_i).$$

Taking the sample s_i as input, the prediction function $h(s_i; \mathbf{x})$ parameterized by the model parameter $\mathbf{x} \in \mathbb{R}^d$ together with the sample label y_i constitute the input of loss function $\ell(h(s_i; \mathbf{x}), y_i)$, which represents the loss caused by the model parameter \mathbf{x} at the i -th sample label-pair (s_i, y_i) . The total empirical loss $f(\mathbf{x})$ is defined as the arithmetic mean of losses of all sample label-pairs, $\frac{1}{n} \sum_{i=1}^n f_i(\mathbf{x})$.

Traditionally, the optimization procedure aims to attain the most suitable model parameter w_* through a numerical iterative algorithm that minimizes the empirical loss on the training set. However, in various cases, such a model parameter w_* does not yield a satisfactory test accuracy on the test dataset while leading the loss landscape with sharp local minima and leaving the model with poor generalization performance.

Therefore, given narrowing the generalization gap, inspired by the adaptive regularization method in [1, 3] and the definition of sharpness in [6], letting $R(\mathbf{x}) = \max_{\|\epsilon\| \leq \rho} f(\mathbf{x} + \epsilon) - f(\mathbf{x})$, the objective function in our proposed SAM with adaptive regularization parameter (SAMAR) is defined as follows

$$\min_{\mathbf{x} \in \mathbb{R}^d} f(\mathbf{x}) + \lambda R(\mathbf{x}) = \min_{\mathbf{x} \in \mathbb{R}^d} \max_{\|\epsilon\| \leq \rho} (1 - \lambda) f(\mathbf{x}) + \lambda f(\mathbf{x} + \epsilon), \quad (1)$$

where ρ is the radius of the neighborhood near \mathbf{x} . Apparently $\min_{\mathbf{x} \in \mathbb{R}^d} f(\mathbf{x}) + \lambda R(\mathbf{x})$ represents a trade-off between minimization loss and sharpness reduction. We not only emphasize reducing the training loss as much as possible but also consider strengthening the model generalization performance. The regularization parameter λ reflects the importance placed on the generalization capability.

Next, consider the internal maximization procedure of (1). Let $\epsilon_{\mathbf{x}_k}$ represent the maximal point of the internal maximization problem at k -th step \mathbf{x}_k . Then, the following consequences could be derived

$$\begin{aligned} \epsilon_{\mathbf{x}_k} &\triangleq \arg \max_{\|\epsilon\| \leq \rho} (1 - \lambda_k) f(\mathbf{x}_k) + \lambda_k f(\mathbf{x}_k + \epsilon) \\ &\stackrel{(\star)}{\approx} \arg \max_{\|\epsilon\| \leq \rho} \lambda_k [f(\mathbf{x}_k) + \nabla f(\mathbf{x}_k)^T \epsilon] \\ &\stackrel{(\Delta)}{\approx} \arg \max_{\|\epsilon\| \leq \rho} \lambda_k [f(\mathbf{x}_k) + \mathbf{g}(\mathbf{x}_k)^T \epsilon], \\ &\Rightarrow \epsilon_{\mathbf{x}_k} = \rho \frac{\mathbf{g}(\mathbf{x}_k)}{\|\mathbf{g}(\mathbf{x}_k)\|}, \end{aligned}$$

where (\star) is first-order approximated via expanding $f(\mathbf{x}_k + \epsilon)$ at \mathbf{x}_k with Taylor’s formula. (Δ) is approximated by utilizing the stochastic gradient of the sample $\mathbf{g}(\mathbf{x}_k)$ instead of the full gradient $\nabla f(\mathbf{x}_k)$. This result of adversary perturbation aligns with [15, 17, 18]. Thus, referring to the optimization process of SGD and SAM, our object function (1) is equivalent to solving the following minimization problem (2) ($\epsilon_{\mathbf{x}} = \rho \frac{\mathbf{g}(\mathbf{x})}{\|\mathbf{g}(\mathbf{x})\|}$, $\mathbf{x} \in \{\mathbf{x}_0, \mathbf{x}_1, \dots, \mathbf{x}_{K-1}\}$). Then, the process of the SAMAR algorithm can be described as Algorithm 1.

$$f(\mathbf{x}) + \lambda_k R(\mathbf{x}) \approx (1 - \lambda_k) f(\mathbf{x}) + \lambda_k f(\mathbf{x} + \epsilon_{\mathbf{x}}). \quad (2)$$

The initialization of hyperparameters $(\lambda_0, \chi, \gamma, \dots)$, the random sampling and adversary perturbation calculation in steps 1-2 are ordinary. The parameter of the model \mathbf{x}_{k+1} is updated iteratively utilizing gradient descent in steps 3-4. Steps 5-6 capture the adaptive update rule for the regularization parameter λ_{k+1} . In Algorithm 1, χ represents the threshold for the ratio of the recent sharpness to the previous one. γ restricts the amplitude of the adaptive adjustment to λ_{k+1} . $\text{Proj}_{[\delta, 1-\delta]}(\cdot) \triangleq \max(\delta, \min(\cdot, 1 - \delta))$ denotes a projection operation, which constrains the range of λ_{k+1} to $[\delta, 1 - \delta]$.

Adaptive Regularization Parameter Strategy. Our work builds upon previous adaptive regularization strategies introduced by [1, 3], with a focus on dynamically adjusting the regularization parameter λ based on sharpness changes during the optimization procedure. The core of our strategy is centred around the following ratio:

$$\begin{aligned} r_k &\triangleq \frac{|f(\mathbf{x}_k + \epsilon_{\mathbf{x}_k}) - f(\mathbf{x}_k)|}{|f(\mathbf{x}_{k-1} + \epsilon_{\mathbf{x}_{k-1}}) - f(\mathbf{x}_{k-1})|} \\ &\approx \frac{|\langle \mathbf{g}(\mathbf{x}_k), \epsilon_{\mathbf{x}_k} \rangle|}{|\langle \mathbf{g}(\mathbf{x}_{k-1}), \epsilon_{\mathbf{x}_{k-1}} \rangle|} = \frac{\|\mathbf{g}(\mathbf{x}_k)\|}{\|\mathbf{g}(\mathbf{x}_{k-1})\|}, \end{aligned}$$

which serves as a measure of how much the local sharpness changes. If r_k becomes significantly larger than 1, this indicates that the optimization process has moved into a

Algorithm 1 Sharpness Aware Minimization with Adaptive Regularization

Initialize: $\mathbf{x}_0, \rho, \eta_0, 0 < \lambda_0 < 1, \chi, \gamma > 1, 0 < \delta < 1$.
for $k = 0, \dots, K - 1$ **do**
step 1: Compute the stochastic gradient $\mathbf{g}(\mathbf{x}_k)$ on the batch data.
step 2: Calculate $\epsilon_{\mathbf{x}_k} = \rho \frac{\mathbf{g}(\mathbf{x}_k)}{\|\mathbf{g}(\mathbf{x}_k)\|}$ through first-order stochastic linearization approximation.
step 3: Let $\mathbf{s}_k = (1 - \lambda_k)\mathbf{g}(\mathbf{x}_k) + \lambda_k\mathbf{g}(\mathbf{x}_k + \epsilon_{\mathbf{x}_k})$.
step 4: $\mathbf{x}_{k+1} = \mathbf{x}_k - \eta_k \mathbf{s}_k$.
step 5: Calculate $r_k = \frac{\|\mathbf{g}(\mathbf{x}_k)\|}{\|\mathbf{g}(\mathbf{x}_{k-1})\|}$.
step 6:
 if $r_k \geq \chi$ or $k = 0$: $\lambda_{k+1} = \mathbf{Proj}_{[\delta, 1-\delta]}(\gamma \lambda_k)$.
 else : $\lambda_{k+1} = \mathbf{Proj}_{[\delta, 1-\delta]}(\frac{1}{\gamma} \lambda_k)$.
step 7: $k = k + 1$.
end for
return \mathbf{x}_K

sharper region of the loss surface. In such cases, increasing the regularization parameter λ is necessary to counteract the sharpness and encourage the algorithm to find flatter minima, which generally leads to better generalization performance. On the other hand, if r_k becomes much smaller than 1, the algorithm has entered a flatter region. In this scenario, reducing λ allows the algorithm to focus more on minimizing the primary objective function. This ensures that the model can fit the sample data more effectively without being overly constrained by the regularization term.

B. Convergence Analysis

In this subsection, the convergence analysis process of Algorithm 1 will be performed to deduce its rate of convergence. Before we start, the following assumptions are outlined, which are pretty common in the general algorithm convergence analysis process.

Assumption 1 (Lower Bound.) $f(\mathbf{x})$ has a lower bound f_{\inf} , i.e., $f(\mathbf{x}) \geq f_{\inf} > -\infty \forall \mathbf{x} \in \mathbb{R}^d$, which means that the optimal value of $f(\mathbf{x})$ exists.

Assumption 2 (Lipschitz Gradient.) $f(\mathbf{x})$ is continuously differentiable and $\nabla f(\mathbf{x})$ satisfies the Lipschitz condition. Namely, there exists a positive constant $L > 0$ and $\|\nabla f(\mathbf{x}) - \nabla f(\mathbf{y})\| \leq L\|\mathbf{x} - \mathbf{y}\|, \|\mathbf{g}(\mathbf{x}) - \mathbf{g}(\mathbf{y})\| \leq L\|\mathbf{x} - \mathbf{y}\|, \forall \mathbf{x}, \mathbf{y} \in \mathbb{R}^d$.

Assumption 3 (Bounded Variance.) The stochastic gradient of the sample $\mathbf{g}(\mathbf{x}_k)$ is the unbiased estimation of $\nabla f(\mathbf{x}_k)$ and the variance of $\mathbf{g}(\mathbf{x}_k)$ exists, i.e., $\mathbb{E}[\mathbf{g}(\mathbf{x}_k)] = \nabla f(\mathbf{x}_k), \mathbb{E}[\|\mathbf{g}(\mathbf{x}_k) - \nabla f(\mathbf{x}_k)\|^2] \leq \sigma^2$, for some constant $\sigma > 0$.

Theorem 1 (Convergence Results of SAMAR.) Under the Assumptions 1-3, ρ and ν satisfy $\rho = \frac{\rho_0}{\sqrt{K}}, \nu = 1 - \frac{5L\eta_0}{2\sqrt{K}}$, for the sequence $\{\mathbf{x}_k\}_{k \geq 0}$ generated by Algorithm 1 run with a

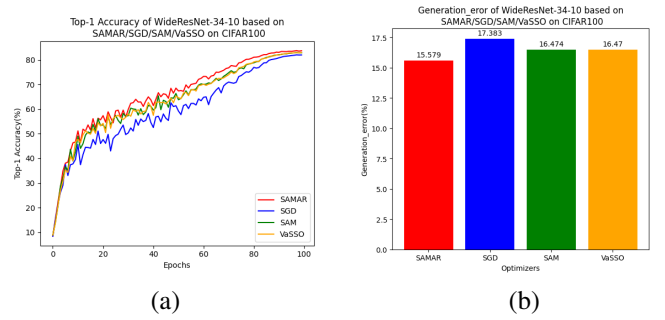


Fig. 1. (a) Epochs vs. Top-1 accuracy obtained from WideResNet-34-10 for CIFAR-100 classification by utilizing different optimizers; (b) Generation_error of WideResNet-34-10 based on different optimizers on CIFAR-100.

learning rate $\eta_k = \frac{\eta_0}{\sqrt{K}} \leq \frac{2}{5L}$. Then it holds that

$$\begin{aligned} & \frac{1}{K} \sum_{k=0}^{K-1} \mathbb{E}[\|\nabla f(\mathbf{x}_k)\|^2] \\ & \leq \frac{1}{\nu} \left[\frac{f(\mathbf{x}_0) - f_{\inf}}{\eta_0 \sqrt{K}} + \frac{L\rho_0^2}{2\eta_0 \sqrt{K}} + \frac{3L\eta_0\sigma^2}{\sqrt{K}} + \frac{2L^3\eta_0\rho_0^2}{K^{\frac{3}{2}}} \right], \end{aligned}$$

and

$$\begin{aligned} \frac{1}{K} \sum_{k=0}^{K-1} \mathbb{E}[\|\nabla f(\mathbf{x}_k + \epsilon_{\mathbf{x}_k})\|^2] & \leq \frac{2}{\nu} \left[\frac{f(\mathbf{x}_0) - f_{\inf}}{\eta_0 \sqrt{K}} + \frac{L\rho_0^2}{2\eta_0 \sqrt{K}} \right. \\ & \quad \left. + \frac{3L\eta_0\sigma^2}{\sqrt{K}} + \frac{2L^3\eta_0\rho_0^2}{K^{\frac{3}{2}}} \right] + \frac{2L^2\rho_0^2}{K}. \end{aligned}$$

Theorem 1 indicates that the SAMAR algorithm exhibits a sublinear convergence rate $\mathcal{O}(\frac{1}{\sqrt{K}})$, which is consistent with SGD. The detailed proof of Theorem 1 can be found in the Appendix¹. Notably, our proof does not require the more restrictive assumption of bounded gradient compared to the literature [7, 15, 18, 19].

III. NUMERICAL EXPERIMENTS

In this section, in order to verify that SAMAR performs well in improving the model generalization, we conduct a series of experiments to compare SAMAR with SGD, SAM and VaSSO optimizers in terms of effectiveness and model generalization. The code can be found at the same link as the Appendix.

A. Models, Benchmark Datasets and Metrics

CIFAR-10 and CIFAR-100 are widely recognized benchmarks, allowing for fair comparison with existing methods. Hence we train ResNet-34 [8] and WideResNet-34-10 [25] neural network models on CIFAR-10 and CIFAR-100 datasets. Meanwhile, five evaluation metrics are recorded: the maximum of top-1 accuracy and the maximum of top-5 accuracy on the test dataset during 100 epochs, the average of top-1 accuracy for the last ten epochs on the test and train datasets, and generalization error. They are denoted as Top-1, Top-5, Last10_Top-1_Test, Last10_Top-1_Train, and Generation_Error in order of precedence, where Generation_Error is computed

¹See <https://github.com/JinpingZou/SAMAR/tree/main>.

TABLE I
COMPARISON OF 5 EVALUATION METRICS (%) FOR RESNET-34 AND WIDERESNET-34-10 USING SAMAR, SGD, SAM, AND VASSO ON CIFAR-10

| CIFAR-10 | Metrics | SAMAR | SGD | SAM | VaSSO |
|------------------|--------------------|---------------------------------------|--------------------------------|---------------------------------------|---------------------------------------|
| ResNet-34 | Top-1 | 96.370 _{96.297±0.054} | 95.730 _{95.640±0.067} | 96.190 _{96.147±0.037} | 96.500 _{96.320±0.131} |
| | Top-5 | 99.950 _{99.943±0.005} | 99.950 _{99.933±0.017} | 99.960 _{99.953±0.005} | 99.990 _{99.973±0.012} |
| | Last10_Top-1_Test | 96.184 _{96.117±0.058} | 95.414 _{95.328±0.062} | 96.059 _{96.020±0.028} | 96.037 _{96.179±0.103} |
| | Last10_Top-1_Train | 98.802 _{98.742±0.043} | 98.551 _{98.504±0.054} | 98.840 _{98.829±0.008} | 98.820 _{98.759±0.085} |
| | Generation_Error | 2.665 _{2.625±0.031} | 3.234 _{3.177±0.041} | 2.839 _{2.809±0.031} | 2.646 _{2.580±0.055} |
| WideResNet-34-10 | Top-1 | 97.010 _{96.963±0.034} | 96.600 _{96.530±0.051} | 96.890 _{96.837±0.075} | 96.940 _{96.913±0.021} |
| | Top-5 | 99.980 _{99.973±0.005} | 99.960 _{99.953±0.005} | 99.980 _{99.973±0.009} | 99.980 _{99.977±0.005} |
| | Last10_Top-1_Test | 96.947 _{96.874±0.053} | 96.524 _{96.444±0.057} | 96.839 _{96.777±0.071} | 96.863 _{96.834±0.025} |
| | Last10_Top-1_Train | 99.420 _{99.407±0.011} | 99.400 _{99.388±0.009} | 99.420 _{99.417±0.004} | 99.424 _{99.417±0.006} |
| | Generation_Error | 2.572 _{2.534±0.051} | 2.987 _{2.944±0.057} | 2.734 _{2.640±0.067} | 2.615 _{2.583±0.028} |

TABLE II
COMPARISON OF 5 EVALUATION METRICS (%) FOR RESNET-34 AND WIDERESNET-34-10 USING SAMAR, SGD, SAM, AND VASSO ON CIFAR-100

| CIFAR-100 | Metrics | SAMAR | SGD | SAM | VaSSO |
|------------------|--------------------|---------------------------------------|--------------------------------|--------------------------------|--------------------------------|
| ResNet-34 | Top-1 | 79.980 _{79.633±0.256} | 78.070 _{77.707±0.507} | 79.220 _{79.027±0.148} | 79.690 _{79.350±0.453} |
| | Top-5 | 95.510 _{95.347±0.117} | 94.650 _{94.490±0.199} | 95.380 _{95.253±0.111} | 95.440 _{95.253±0.257} |
| | Last10_Top-1_Test | 79.564 _{79.270±0.235} | 77.841 _{77.401±0.509} | 78.912 _{78.763±0.141} | 79.285 _{78.999±0.398} |
| | Last10_Top-1_Train | 98.281 _{98.221±0.067} | 97.669 _{97.613±0.040} | 98.456 _{98.412±0.040} | 98.467 _{98.419±0.041} |
| | Generation_Error | 19.265 _{18.951±0.291} | 20.981 _{20.211±0.549} | 19.785 _{19.649±0.101} | 19.931 _{19.420±0.361} |
| WideResNet-34-10 | Top-1 | 83.770 _{83.753±0.024} | 82.360 _{82.023±0.248} | 83.010 _{82.983±0.021} | 83.020 _{82.980±0.029} |
| | Top-5 | 96.970 _{96.840±0.092} | 96.070 _{95.930±0.104} | 96.590 _{96.487±0.101} | 96.600 _{96.527±0.057} |
| | Last10_Top-1_Test | 83.490 _{83.468±0.025} | 81.911 _{81.599±0.223} | 82.631 _{82.605±0.031} | 82.722 _{82.631±0.069} |
| | Last10_Top-1_Train | 99.020 _{99.012±0.006} | 98.791 _{98.780±0.010} | 99.035 _{99.027±0.008} | 99.040 _{99.025±0.012} |
| | Generation_Error | 15.579 _{15.545±0.026} | 17.383 _{17.180±0.217} | 16.474 _{16.421±0.037} | 16.470 _{16.395±0.077} |

by differencing Last10_Top-1_Train with Last10_Top-1_Test. The experimental data in all tables are obtained after three independent runs. The best values for the four metrics related to the test dataset and generalization performance are bolded, and the data format is $\max_{\text{mean} \pm \text{std}}$.

B. Implementation

We train ResNet-34 and WideResNet34-10 for 100 epochs on CIFAR-10 and CIFAR-100 with a batch size of 256. To strengthen the model’s capacity for feature learning, we perform data augmentation through normalization, cutout, random cropping and random horizontal flip. To accelerate the speed of convergence of the training process, a learning rate scheduling strategy is adopted during the training process. This scheduling strategy is specified by decaying the learning rate with a CosineAnneal strategy between different epochs and maintaining the same learning rate between different batches of the same epoch. For additional hyperparameters setting, please refer to Table III in the Appendix for detail. All experiments are performed on a single NVIDIA RTX 4090D GPU.

C. Analysis of Results

CIFAR-10. As in the case of the data shown in Table I, SAMAR outperforms SAM and SGD in almost all the best values for the four metrics relative to the test data set and generalization performance, provided that the models used are identical. In comparison, the main reason that SAMAR does not perform as well as VaSSO on some metrics is that the scale of CIFAR-10 dataset is relatively small, therefore the models are easily overfitted and do not tend to apparently reflect the performance gap between different optimizers.

CIFAR-100. Based on the results of the experiment in Table II, we can conclude that SAMAR outperforms SAM and VaSSO, especially compared to the SGD optimizer when training the ResNet-34 and WideResNet-34-10 models. Specifically, SAMAR achieves a significant improvement in classification accuracy. In addition, it shows better control of the generalization error, which indicates that SAMAR strengthens the generalization ability of the models while improving their performance. The Top-1 accuracy of SAMAR is about 0.7% higher than SAM and VaSSO, and the Generalization_Error is about 0.9% lower than SAM and VaSSO. The variation of Top-1 accuracy with iterative epochs when training WideResNet-34-10 on CIFAR-100 using different optimizers separately is shown in Fig. 1 (a), while the Generalization_Error is shown in Fig. 1 (b). Both subfigures illustrate that the usage of SAMAR can produce higher performance gains and stronger generalization ability when training slightly large models on relatively complex datasets.

IV. CONCLUSIONS

This paper presents SAMAR, a novel algorithm featuring adaptively adjustable the regularization parameter λ . Although the convergence rate of SAMAR is theoretically aligned with that of SAM, empirical results on CIFAR-10 and CIFAR-100 datasets demonstrate that SAMAR consistently achieves higher accuracy and superior generalization, especially for larger models on complex datasets. However, we acknowledge that SAMAR may lag behind VaSSO in certain scenarios. Our future work will focus on enhancing the updating mechanisms for adversarial perturbations to further improve generalization performance.

REFERENCES

- [1] Naman Agarwal, Nicolas Boumal, Brian Bullins, and Coralia Cartis. Adaptive regularization with cubics on manifolds. *Mathematical Programming*, 188:85–134, 2021.
- [2] Maksym Andriushchenko and Nicolas Flammarion. Towards understanding sharpness-aware minimization. In *International Conference on Machine Learning*, pages 639–668. PMLR, 2022.
- [3] Stefania Bellavia and Gianmarco Gurioli. Stochastic analysis of an adaptive cubic regularization method under inexact gradient evaluations and dynamic hessian accuracy. *Optimization*, 71(1):227–261, 2022.
- [4] Léon Bottou, Frank E Curtis, and Jorge Nocedal. Optimization methods for large-scale machine learning. *SIAM review*, 60(2):223–311, 2018.
- [5] Jiawei Du, Hanshu Yan, Jiashi Feng, Joey Tianyi Zhou, Liangli Zhen, Rick Siow Mong Goh, and Vincent Y. F. Tan. Efficient sharpness-aware minimization for improved training of neural networks. In *The Tenth International Conference on Learning Representations, ICLR 2022, Virtual Event, April 25-29, 2022*.
- [6] Pierre Foret, Ariel Kleiner, Hossein Mobahi, and Behnam Neyshabur. Sharpness-aware minimization for efficiently improving generalization. In *9th International Conference on Learning Representations, ICLR 2021, Virtual Event, Austria, May 3-7, 2021*.
- [7] Igor Gitman, Hunter Lang, Pengchuan Zhang, and Lin Xiao. Understanding the role of momentum in stochastic gradient methods. *Advances in Neural Information Processing Systems*, 32, 2019.
- [8] Kaiming He, Xiangyu Zhang, Shaoqing Ren, and Jian Sun. Deep residual learning for image recognition. In *Proceedings of the IEEE Conference on Computer Vision and Pattern Recognition (CVPR)*, June 2016.
- [9] Yiding Jiang, Behnam Neyshabur, Hossein Mobahi, Dilip Krishnan, and Samy Bengio. Fantastic generalization measures and where to find them. In *8th International Conference on Learning Representations, ICLR 2020, Addis Ababa, Ethiopia, April 26-30, 2020*.
- [10] Nitish Shirish Keskar, Dheevatsa Mudigere, Jorge Nocedal, Mikhail Smelyanskiy, and Ping Tak Peter Tang. On large-batch training for deep learning: Generalization gap and sharp minima. In *5th International Conference on Learning Representations, ICLR 2017, Toulon, France, April 24-26, 2017, Conference Track Proceedings*, 2017.
- [11] Pham Duy Khanh, Hoang-Chau Luong, Boris S Morukhovich, and Dat Ba Tran. Fundamental convergence analysis of sharpness-aware minimization. *arXiv preprint arXiv:2401.08060*, 2024.
- [12] Jonas Moritz Kohler and Aurelien Lucchi. Sub-sampled cubic regularization for non-convex optimization. In *International Conference on Machine Learning*, pages 1895–1904. PMLR, 2017.
- [13] Jungmin Kwon, Jeongseop Kim, Hyunseo Park, and In Kwon Choi. Asam: Adaptive sharpness-aware minimization for scale-invariant learning of deep neural networks. In *International Conference on Machine Learning*, pages 5905–5914. PMLR, 2021.
- [14] Bingcong Li and Georgios B. Giannakis. Enhancing sharpness-aware optimization through variance suppression. In *Advances in Neural Information Processing Systems 36: Annual Conference on Neural Information Processing Systems, NeurIPS 2023, New Orleans, LA, USA, December 10 - 16, 2023*.
- [15] Tao Li, Pan Zhou, Zhengbao He, Xinwen Cheng, and Xiaolin Huang. Friendly sharpness-aware minimization. In *Proceedings of the IEEE/CVF Conference on Computer Vision and Pattern Recognition*, pages 5631–5640, 2024.
- [16] Xiaoyu Li, Zhenxun Zhuang, and Francesco Orabona. A second look at exponential and cosine step sizes: Simplicity, adaptivity, and performance. In *International Conference on Machine Learning*, pages 6553–6564. PMLR, 2021.
- [17] Yong Liu, Siqi Mai, Xiangning Chen, Cho-Jui Hsieh, and Yang You. Towards efficient and scalable sharpness-aware minimization. In *Proceedings of the IEEE/CVF Conference on Computer Vision and Pattern Recognition (CVPR)*, pages 12360–12370, June 2022.
- [18] Peng Mi, Li Shen, Tianhe Ren, Yiyi Zhou, Xiaoshuai Sun, Rongrong Ji, and Dacheng Tao. Make sharpness-aware minimization stronger: A sparsified perturbation approach. *Advances in Neural Information Processing Systems*, 35:30950–30962, 2022.
- [19] Hao Sun, Li Shen, Qihuang Zhong, Liang Ding, Shixiang Chen, Jingwei Sun, Jing Li, Guangzhong Sun, and Dacheng Tao. Adasam: Boosting sharpness-aware minimization with adaptive learning rate and momentum for training deep neural networks. *Neural Networks*, 169:506–519, 2024.
- [20] Tao Sun, Dongsheng Li, and Bao Wang. Adaptive random walk gradient descent for decentralized optimization. In *ICML*, pages 20790–20809. PMLR, 2022.
- [21] Tao Sun, Huaming Ling, Zuoqiang Shi, Dongsheng Li, and Bao Wang. Training deep neural networks with adaptive momentum inspired by the quadratic optimization. *arXiv preprint arXiv:2110.09057*, 2021.
- [22] Tao Sun, Linbo Qiao, Qing Liao, and Dongsheng Li. Novel convergence results of adaptive stochastic gradient descents. *IEEE Transactions on Image Processing*, 30:1044–1056, 2020.
- [23] Tao Sun, Yuejiao Sun, Dongsheng Li, and Qing Liao. General proximal incremental aggregated gradient algorithms: Better and novel results under general scheme. *Advances in Neural Information Processing Systems*, 32, 2019.
- [24] Ziqing Wen, Xiaoge Deng, Tao Sun, and Dongsheng Li. Normalized stochastic heavy ball with adaptive momentum. In *ECAI*, pages 2615–2622, 2023.
- [25] Sergey Zagoruyko. Wide residual networks. *arXiv preprint arXiv:1605.07146*, 2016.

APPENDIX FOR

Sharpness-Aware Minimization with Adaptive Regularization for Training Deep Neural Networks

A. Proof of Theorem 1

A significant conclusion (3) could be deduced from Assumption 2. If $\nabla f(\mathbf{x})$ has a Lipschitz gradient with constant $L > 0$, we have

$$\begin{aligned}
 f(\mathbf{x}_{k+1}) - f(\mathbf{x}_k) &\leq \langle \nabla f(\mathbf{x}_k), \mathbf{x}_{k+1} - \mathbf{x}_k \rangle + \frac{L}{2} \|\mathbf{x}_{k+1} - \mathbf{x}_k\|^2 \\
 &= -\eta_k \langle \nabla f(\mathbf{x}_k), (1 - \lambda_k)\mathbf{g}(\mathbf{x}_k) + \lambda_k\mathbf{g}(\mathbf{x}_k + \boldsymbol{\epsilon}_{\mathbf{x}_k}) \rangle + \frac{L}{2} \eta_k^2 \|(1 - \lambda_k)\mathbf{g}(\mathbf{x}_k) + \lambda_k\mathbf{g}(\mathbf{x}_k + \boldsymbol{\epsilon}_{\mathbf{x}_k})\|^2 \\
 &= \underbrace{-\eta_k \langle \nabla f(\mathbf{x}_k), (1 - \lambda_k)\mathbf{g}(\mathbf{x}_k) \rangle}_{:=\spadesuit} - \underbrace{\eta_k \langle \nabla f(\mathbf{x}_k), \lambda_k\mathbf{g}(\mathbf{x}_k + \boldsymbol{\epsilon}_{\mathbf{x}_k}) \rangle}_{:=\heartsuit} + \underbrace{\frac{L}{2} \eta_k^2 \|(1 - \lambda_k)\mathbf{g}(\mathbf{x}_k) + \lambda_k\mathbf{g}(\mathbf{x}_k + \boldsymbol{\epsilon}_{\mathbf{x}_k})\|^2}_{:=\clubsuit}.
 \end{aligned} \tag{3}$$

We calculate each of the above three parts respectively

$$\begin{aligned}
 \spadesuit &= -\eta_k \langle \nabla f(\mathbf{x}_k), (1 - \lambda_k)\mathbf{g}(\mathbf{x}_k) \rangle \\
 &= -\eta_k(1 - \lambda_k) [\langle \nabla f(\mathbf{x}_k), \mathbf{g}(\mathbf{x}_k) - \nabla f(\mathbf{x}_k) \rangle] - \eta_k(1 - \lambda_k) \|\nabla f(\mathbf{x}_k)\|^2,
 \end{aligned} \tag{4}$$

$$\begin{aligned}
 \heartsuit &= -\eta_k \langle \nabla f(\mathbf{x}_k), \lambda_k\mathbf{g}(\mathbf{x}_k + \boldsymbol{\epsilon}_{\mathbf{x}_k}) \rangle \\
 &= -\eta_k \lambda_k \langle \nabla f(\mathbf{x}_k), \mathbf{g}(\mathbf{x}_k + \boldsymbol{\epsilon}_{\mathbf{x}_k}) - \mathbf{g}(\mathbf{x}_k) \rangle - \eta_k \lambda_k \langle \nabla f(\mathbf{x}_k), \mathbf{g}(\mathbf{x}_k) - \nabla f(\mathbf{x}_k) \rangle - \eta_k \lambda_k \|\nabla f(\mathbf{x}_k)\|^2 \\
 &\stackrel{(a)}{\leq} \eta_k \lambda_k L \rho \|\nabla f(\mathbf{x}_k)\| - \eta_k \lambda_k \|\nabla f(\mathbf{x}_k)\|^2 - \eta_k \lambda_k \langle \nabla f(\mathbf{x}_k), \mathbf{g}(\mathbf{x}_k) - \nabla f(\mathbf{x}_k) \rangle,
 \end{aligned} \tag{5}$$

$$\begin{aligned}
 \clubsuit &= \frac{L}{2} \eta_k^2 \|(1 - \lambda_k)\mathbf{g}(\mathbf{x}_k) + \lambda_k\mathbf{g}(\mathbf{x}_k + \boldsymbol{\epsilon}_{\mathbf{x}_k})\|^2 \\
 &\stackrel{(b)}{\leq} L \eta_k^2 [(1 - \lambda_k)^2 \|\mathbf{g}(\mathbf{x}_k)\|^2 + \lambda_k^2 \|\mathbf{g}(\mathbf{x}_k + \boldsymbol{\epsilon}_{\mathbf{x}_k})\|^2],
 \end{aligned} \tag{6}$$

where the inequality (a) uses Lipschitz continuity $\|\mathbf{g}(\mathbf{x}_k + \boldsymbol{\epsilon}_{\mathbf{x}_k}) - \mathbf{g}(\mathbf{x}_k)\| \leq L \|\boldsymbol{\epsilon}_{\mathbf{x}_k}\|$ and the Cauchy's inequality $\langle \mathbf{x}, \mathbf{y} \rangle \leq \|\mathbf{x}\| \cdot \|\mathbf{y}\|$. The inequality (b) depends on the inequality $\|\mathbf{a} + \mathbf{b}\|^2 \leq 2\|\mathbf{a}\|^2 + 2\|\mathbf{b}\|^2$. Taking expectation on (4), (5) and (6), we can further get

$$\mathbb{E}[\spadesuit] \stackrel{(c)}{=} -\eta_k(1 - \lambda_k) \mathbb{E}[\|\nabla f(\mathbf{x}_k)\|^2], \tag{7}$$

$$\begin{aligned}
 \mathbb{E}[\heartsuit] &\leq \eta_k \lambda_k L \rho \mathbb{E}[\|\nabla f(\mathbf{x}_k)\|] - \eta_k \lambda_k \mathbb{E}[\|\nabla f(\mathbf{x}_k)\|^2] \\
 &\stackrel{(d)}{\leq} \frac{L}{2} \rho^2 + \frac{L}{2} \eta_k^2 \lambda_k^2 [\mathbb{E}[\|\nabla f(\mathbf{x}_k)\|]]^2 - \eta_k \lambda_k \mathbb{E}[\|\nabla f(\mathbf{x}_k)\|^2] \\
 &\stackrel{(e)}{\leq} \frac{L}{2} \rho^2 + \frac{L}{2} \eta_k^2 \lambda_k^2 \mathbb{E}[\|\nabla f(\mathbf{x}_k)\|^2] - \eta_k \lambda_k \mathbb{E}[\|\nabla f(\mathbf{x}_k)\|^2],
 \end{aligned} \tag{8}$$

$$\begin{aligned}
 \mathbb{E}[\clubsuit] &\leq L \eta_k^2 [(1 - \lambda_k)^2 \mathbb{E}[\|\mathbf{g}(\mathbf{x}_k)\|^2] + \lambda_k^2 \mathbb{E}[\|\mathbf{g}(\mathbf{x}_k + \boldsymbol{\epsilon}_{\mathbf{x}_k})\|^2]] \\
 &\stackrel{(f)}{\leq} L \eta_k^2 [(1 - \lambda_k)^2 (\sigma^2 + \mathbb{E}[\|\nabla f(\mathbf{x}_k)\|^2]) + \lambda_k^2 (2L^2 \rho^2 + 2\sigma^2 + 2\mathbb{E}[\|\nabla f(\mathbf{x}_k)\|^2])],
 \end{aligned} \tag{9}$$

where the equality (c) utilizes that $\mathbf{g}(\mathbf{x}_k)$ is the unbiased estimation of $\nabla f(\mathbf{x}_k)$. The inequality (d) leverages the basic inequality $\frac{a+b}{2} \geq \sqrt{ab}$. The inequality (e) comes from the nonnegative variance property $\text{Var}(\mathbf{X}) = \mathbb{E}[\mathbf{X}^2] - [\mathbb{E}[\mathbf{X}]]^2 \geq 0$. A combination of the following results (11) and (13) leads to (f). After a simple mathematical derivation of $\|\mathbf{g}(\mathbf{x}_k)\|^2$, the following results could be derived:

$$\begin{aligned}
 \|\mathbf{g}(\mathbf{x}_k)\|^2 &= \|\mathbf{g}(\mathbf{x}_k) - \nabla f(\mathbf{x}_k) + \nabla f(\mathbf{x}_k)\|^2 \\
 &= \|\mathbf{g}(\mathbf{x}_k) - \nabla f(\mathbf{x}_k)\|^2 + \|\nabla f(\mathbf{x}_k)\|^2 + 2\langle \mathbf{g}(\mathbf{x}_k) - \nabla f(\mathbf{x}_k), \nabla f(\mathbf{x}_k) \rangle.
 \end{aligned} \tag{10}$$

Taking expectation on (10), then we derive

$$\mathbb{E}[\|\mathbf{g}(\mathbf{x}_k)\|^2] \leq \sigma^2 + \mathbb{E}[\|\nabla f(\mathbf{x}_k)\|^2]. \tag{11}$$

After a plain derivation of $\|\mathbf{g}(\mathbf{x}_k + \boldsymbol{\epsilon}_{\mathbf{x}_k})\|^2$, we have

$$\begin{aligned}\|\mathbf{g}(\mathbf{x}_k + \boldsymbol{\epsilon}_{\mathbf{x}_k})\|^2 &= \|\mathbf{g}(\mathbf{x}_k + \boldsymbol{\epsilon}_{\mathbf{x}_k}) - \mathbf{g}(\mathbf{x}_k) + \mathbf{g}(\mathbf{x}_k)\|^2 \\ &\leq 2\|\mathbf{g}(\mathbf{x}_k + \boldsymbol{\epsilon}_{\mathbf{x}_k}) - \mathbf{g}(\mathbf{x}_k)\|^2 + 2\|\mathbf{g}(\mathbf{x}_k)\|^2 \\ &\leq 2L^2\rho^2 + 2\|\mathbf{g}(\mathbf{x}_k)\|^2.\end{aligned}\quad (12)$$

Taking expectation on (12) gives us

$$\mathbb{E}[\|\mathbf{g}(\mathbf{x}_k + \boldsymbol{\epsilon}_{\mathbf{x}_k})\|^2] \leq 2L^2\rho^2 + 2\mathbb{E}[\|\mathbf{g}(\mathbf{x}_k)\|^2]. \quad (13)$$

Taking expectation on (3) and utilizing the results of (7), (8), (9), (11) and (13), we can get

$$\begin{aligned}\mathbb{E}[f(\mathbf{x}_{k+1}) - f(\mathbf{x}_k)] &\leq \mathbb{E}[\spadesuit] + \mathbb{E}[\heartsuit] + \mathbb{E}[\clubsuit] \\ &\leq -\eta_k(1 - \lambda_k)\mathbb{E}[\|\nabla f(\mathbf{x}_k)\|^2] + \frac{L}{2}\rho^2 + \frac{L}{2}\eta_k^2\lambda_k^2\mathbb{E}[\|\nabla f(\mathbf{x}_k)\|^2] - \eta_k\lambda_k\mathbb{E}[\|\nabla f(\mathbf{x}_k)\|^2] \\ &\quad + L\eta_k^2\left[(1 - \lambda_k)^2(\sigma^2 + \mathbb{E}[\|\nabla f(\mathbf{x}_k)\|^2]) + \lambda_k^2(2L^2\rho^2 + 2\sigma^2 + 2\mathbb{E}[\|\nabla f(\mathbf{x}_k)\|^2])\right].\end{aligned}\quad (14)$$

Rearranging these terms and dividing the constant η_k on both sides of (14) yields

$$\begin{aligned}\underbrace{\left[1 - \frac{5}{2}L\eta_k\lambda_k^2 - L\eta_k(1 - \lambda_k)^2\right]}_{:=M_k}\mathbb{E}[\|\nabla f(\mathbf{x}_k)\|^2] &\leq 2L\eta_k\lambda_k^2\sigma^2 + \frac{L\rho^2}{2\eta_k} + L\eta_k(1 - \lambda_k)^2\sigma^2 \\ &\quad + 2L^3\eta_k\lambda_k^2\rho^2 + \frac{\mathbb{E}[f(\mathbf{x}_k) - f(\mathbf{x}_{k+1})]}{\eta_k}.\end{aligned}$$

It holds that $\lambda_k \in (0, 1)$ according to the update rule in Algorithm 1. Thus we have $1 - \frac{5}{2}L\eta_k \leq M_k = 1 - \frac{5}{2}L\eta_k\lambda_k^2 - L\eta_k(1 - \lambda_k)^2 \leq 1 - \frac{5}{7}L\eta_k$, $M_k \geq \nu = 1 - \frac{5L\eta_0}{2\sqrt{K}}$ with $\eta_k = \frac{\eta_0}{\sqrt{K}}$ and $\rho = \frac{\rho_0}{\sqrt{K}}$. Consequently, we further get

$$\begin{aligned}\mathbb{E}[\|\nabla f(\mathbf{x}_k)\|^2] &\leq \frac{1}{\nu}\left[2L\eta_k\sigma^2 + \frac{L\rho^2}{2\eta_k} + L\eta_k\sigma^2 + 2L^3\eta_k\rho^2 + \frac{\mathbb{E}[f(\mathbf{x}_k) - f(\mathbf{x}_{k+1})]}{\eta_k}\right] \\ &= \frac{1}{\nu}\left[\frac{2L\eta_0\sigma^2}{\sqrt{K}} + \frac{L\rho_0^2}{2\eta_0\sqrt{K}} + \frac{L\eta_0\sigma^2}{\sqrt{K}} + \frac{2L^3\eta_0\rho_0^2}{K^{\frac{3}{2}}} + \frac{\mathbb{E}[f(\mathbf{x}_k) - f(\mathbf{x}_{k+1})]}{\eta_0}\sqrt{K}\right].\end{aligned}\quad (15)$$

Summing (15) from $k = 0$ to $K - 1$, we have

$$\begin{aligned}\frac{1}{K}\sum_{k=0}^{K-1}\mathbb{E}[\|\nabla f(\mathbf{x}_k)\|^2] &\leq \frac{1}{\nu}\left[\frac{2L\eta_0\sigma^2}{\sqrt{K}} + \frac{L\rho_0^2}{2\eta_0\sqrt{K}} + \frac{L\eta_0\sigma^2}{\sqrt{K}} + \frac{2L^3\eta_0\rho_0^2}{K^{\frac{3}{2}}} + \frac{\mathbb{E}[f(\mathbf{x}_0) - f(\mathbf{x}_K)]}{\eta_0\sqrt{K}}\right] \\ &\leq \frac{1}{\nu}\left[\frac{f(\mathbf{x}_0) - f_{\inf}}{\eta_0\sqrt{K}} + \frac{L\rho_0^2}{2\eta_0\sqrt{K}} + \frac{3L\eta_0\sigma^2}{\sqrt{K}} + \frac{2L^3\eta_0\rho_0^2}{K^{\frac{3}{2}}}\right].\end{aligned}\quad (16)$$

As to $\frac{1}{K}\sum_{k=0}^{K-1}\mathbb{E}[\|\nabla f(\mathbf{x}_k + \boldsymbol{\epsilon}_{\mathbf{x}_k})\|^2]$, which could be derived by leveraging on (16). After an ordinary derivation of $\|\nabla f(\mathbf{x}_k + \boldsymbol{\epsilon}_{\mathbf{x}_k})\|^2$, we are then led to

$$\begin{aligned}\|\nabla f(\mathbf{x}_k + \boldsymbol{\epsilon}_{\mathbf{x}_k})\|^2 &= \|\nabla f(\mathbf{x}_k + \boldsymbol{\epsilon}_{\mathbf{x}_k}) - \nabla f(\mathbf{x}_k) + \nabla f(\mathbf{x}_k)\|^2 \\ &\leq 2\|\nabla f(\mathbf{x}_k + \boldsymbol{\epsilon}_{\mathbf{x}_k}) - \nabla f(\mathbf{x}_k)\|^2 + 2\|\nabla f(\mathbf{x}_k)\|^2 \\ &\leq 2L^2\rho^2 + 2\|\nabla f(\mathbf{x}_k)\|^2.\end{aligned}\quad (17)$$

Utilizing (17), we have

$$\begin{aligned}\frac{1}{K}\sum_{k=0}^{K-1}\mathbb{E}[\|\nabla f(\mathbf{x}_k + \boldsymbol{\epsilon}_{\mathbf{x}_k})\|^2] &\leq 2L^2\rho^2 + \frac{2}{K}\sum_{k=0}^{K-1}\mathbb{E}[\|\nabla f(\mathbf{x}_k)\|^2] \\ &\leq \frac{2}{\nu}\left[\frac{f(\mathbf{x}_0) - f_{\inf}}{\eta_0\sqrt{K}} + \frac{L\rho_0^2}{2\eta_0\sqrt{K}} + \frac{3L\eta_0\sigma^2}{\sqrt{K}} + \frac{2L^3\eta_0\rho_0^2}{K^{\frac{3}{2}}}\right] + \frac{2L^2\rho_0^2}{K}.\end{aligned}\quad (18)$$

TABLE III
HYPERPARAMETERS SETTING USED TO PRODUCE THE RESULTS OF CIFAR-10/CIFAR-100

| Dataset | Model | Optimizer | Lr | ρ | θ | γ | χ |
|-----------|-------------------|-----------|-----|--------|----------|----------|--------|
| CIFAR-10 | ResNet-34 | SAMAR | 0.3 | 0.10 | - | 1.550 | 1.100 |
| | | SGD | 0.3 | - | - | - | - |
| | | SAM | 0.3 | 0.10 | - | - | - |
| | | VaSSO | 0.3 | 0.10 | 0.9 | - | - |
| | Wide-Resnet-34-10 | SAMAR | 0.1 | 0.10 | - | 1.400 | 1.050 |
| | | SGD | 0.1 | - | - | - | - |
| | | SAM | 0.1 | 0.10 | - | - | - |
| | | VaSSO | 0.1 | 0.10 | 0.9 | - | - |
| CIFAR-100 | ResNet-34 | SAMAR | 0.3 | 0.10 | - | 1.400 | 1.075 |
| | | SGD | 0.3 | - | - | - | - |
| | | SAM | 0.3 | 0.10 | - | - | - |
| | | VaSSO | 0.3 | 0.10 | 0.9 | - | - |
| | Wide-Resnet-34-10 | SAMAR | 0.3 | 0.15 | - | 1.500 | 1.000 |
| | | SGD | 0.3 | - | - | - | - |
| | | SAM | 0.3 | 0.15 | - | - | - |
| | | VaSSO | 0.3 | 0.15 | 0.9 | - | - |

B. Hyperparameters for experiments

The hyperparameters throughout the experiment are noteworthy. Since every model is only trained for 100 epochs, we set a slightly larger initial learning rate to ensure that all models converge after training 100 epochs. Referring to the hyperparameters in the relevant literature [5, 6, 13–15, 18], and combining them with the changes in experimental results we observed while finetuning the hyperparameters, the hyperparameters in experiments are shown in Table III. Following [14], VaSSO adopts $\theta = 0.9$. To reduce the effort of finetuning the hyperparameters, we take $\lambda_0 = 1, \delta = 0.01$ for SAMAR, and weight decay is 0.0005 in all experiments.